Optimal relaxation parameters of DRAMA (dynamic RAMLA) aiming at one-pass image reconstruction for 3D-PET

Eiichi Tanaka[1] and Hiroyuki Kudo[2]

[1] Hamamatsu Photonics KK, Tokyo Branch, Mori-Bldg No 33, Toranomon, Minato-ku, Tokyo, Japan

[2] Department of Computer Science, Graduate School of Systems and Information Engineering, University of Tsukuba, Tsukuba-shi, Ibaraki, Japan

Abstract

We have reported a block-iterative algorithm named as DRAMA for image reconstruction for emission tomography (Tanaka and Kudo 2003). DRAMA is a modified version of the row-action maximum likelihood algorithm (RAMLA), in which the relaxation parameter is subset-dependent and is changed in such a way that the noise propagation from subsets to the reconstructed image is substantially independent of the access order of the subsets. The algorithm provides fast convergence with reasonable signal-to-noise ratio. The optimal relaxation parameter has been derived assuming a two-dimensional (2D)-PET model, and the detailed performance in three-dimensional (3D)-reconstruction has not been clear enough. We have developed the new version "DRAMA-3D," based on the 3D-PET model. The optimal relaxation parameter is a function of access order of the subsets and the ring difference, and its value is determined by simple formulas from the design parameters of the PET scanner, the operating conditions and the post-smoothing resolution. In this paper, we present the theory of DRAMA-3D, the results of simulation studies on the performance of DRAMA-3D and the comparative studies of the related algorithms. It is shown that DRAMA-3D is robust for various access orders of subsets and is suitable to realize the one-pass (single iteration) reconstruction.

1. Introduction

Block iterative algorithms are now important tools for image reconstruction in PET. The best known among these is the ordered subsets EM (OSEM) algorithm (Hudson and Larkin 1994), in which the projection data are grouped into a number of subsets, and the expectation maximization (EM) algorithm (Shepp and Vardi 1982) is applied sequentially to these subsets in turn. A complete cycle of the successive sub-iterations for all subsets forms a main iteration of OSEM. The OSEM algorithm produces remarkable improvements in the initial convergence rate compared to the original EM algorithm by a factor roughly equal to the number of subsets. This property, coupled with the relatively simple form of the update equation, has led to the widespread use of OSEM in PET and SPECT. While the method is practically attractive, it does not converge to the true maximum likelihood (ML) solution but falls into limit cycles, and the excessive acceleration of the convergence by the use of a large number of subsets results in the degradation in signal-to-noise ratio (Hudson and Larkin 1994, Meikle et al 1994).

The drawback of OSEM was improved by incorporating a suitably controlled relaxation parameter denoted by the symbol λ below. The resulting algorithm is called "relaxed OSEM". One example of this approach is the row-action maximum likelihood algorithm (RAMLA) of Browne and De Pierro (1996). RAMLA is a special case of the relaxed OSEM where the number of subsets is equal to the number of projection views. In RAMLA or relaxed OSEM, λ is fixed throughout a complete cycle of sub-iterations. The use of a large λ allows a fast convergence when the data are consistent, but it tends to enhance the error due to inconsistent components (statistical noise) when the data contain Poisson noise. This property prevents the use of single iteration with a large λ, and plural iterations are required with a small λ or with an asymptotically decreasing λ. The undesirable feature on the noise

enhancement with a large λ is due to the fact that the noise components of data are propagated to the final image of the cycle of sub-iterations with different efficiency, and the final image contains more of the noise of the lately accessed projections than those of the early accessed projections.   The unbalanced propagation of the noise is a main cause of the limit cycle phenomenon that degrades the signal-to-noise ratio.

Tanaka and Kudo (2003) have developed an algorithm named as "DRAMA (dynamic RAMLA)", in which λ is "subset-dependent" and is changed in such a way that the noise propagation from subsets to the reconstructed image is substantially independent of the access order of the subsets.   As a result, the contribution of noise from each subset is balanced at the end of each main iteration, making it possible to avoid the limit cycle problem.   We call this property "uniform noise propagation" below.   The algorithm provides fast convergence with reasonable signal-to-noise ratio.   Helou Neto and De Pierro (2005) proved the convergence of DRAMA recently.

The optimal relaxation parameter λ of DRAMA has been derived assuming a 2D-PET model in Tanaka and Kudo (2003), and the detailed performance in 3D-reconstruction has not been well clarified. In spite of these circumstances, DRAMA has been applied successfully to 3D-PET reconstruction (Fukano et al 2004), 3D-PET with list-mode data acquisition (Nakayama and Kudo 2005, Yamada et al 2007) and 2D time-of-flight PET (Tanaka et al 2007).

In this paper, we describe a revised theory of DRAMA for 3D-reconstruction and present the new definitions of the optimal relaxation parameter.   We call the new algorithm "DRAMA-3D" for discriminating it from the previous one, "DRAMA-2D".   This work focuses on the one-pass (single iteration) reconstruction, considering the feature that the number of subsets is usually sufficiently large in the 3D-reconstruction.   The outline of this paper is the following.   In section 2, we describe the theory of the proposed algorithms and the optimal relaxation parameter.   Section 3 describes the simulation studies.   In the last section, we describe a brief discussion of the consequences of our simulation studies and conclusions.

2. Theory

2.1. DRAMA-2D

In this section, we describe briefly the outline of DRAMA based on the 2D-PET model (Tanaka and Kudo 2003), which is necessary in the following revision for 3D-PET model.   Suppose we count coincidences along I lines of response (LORs) and denote by y_i ($1 \leq i \leq I$) the number of detected events along the ith LOR.   These data are arranged into M angular views with the view index m ($1 \leq m \leq M$).   Each view consists of N parallel LORs, where $I = M{\times}N$.   We consider a square image matrix of $N{\times}N = J$ pixels, and photon emission from pixel j is denoted by x_j ($1 \leq j \leq J$).   Effect of the photon attenuation and scattering is not taken into account for simplicity.   The update equations of DRAMA-2D are

$$x_j^{(k,q+1)} = x_j^{(k,q)} + \lambda_k(q)\frac{x_j^{(k,q)}}{C_j}\sum_{i \in S_q} a_{ij}\left(\frac{y_i}{\sum_{j'=1}^{J} a_{ij'}\, x_{j'}^{(k,q)}} - 1\right) \tag{1.1}$$

$$x_j^{(k+1,0)} = x_j^{(k,M)} \tag{1.2}$$

$$C_j = \max_q \sum_{i \in S_q} a_{ij} \tag{1.3}$$

where a_{ij} is the probability that a photon emission from pixel j is recorded in the ith LOR, q (0, 1,$\cdots$, M–1) is the index of the access order of views, and S_q is the subset of LORs accessed at the qth order.   Note that, in DRAMA-2D, the number of subsets is equal to M, and a subset consists of all parallel LORs having a constant view angle.   The index k (0, 1, 2, $\cdots$) refers to the main iterations, $\lambda_k(q)$ is the relaxation parameter ($0 < \lambda_k(q) \leq 1$), and C_j is called the normalization constant.   We assume that the iteration starts with a positive image $x_j^{(0)} > 0$.   To regularize the reconstructed image, we apply the post-

smoothing with a Gaussian filter after the iterations are terminated (Snyder and Miller 1985).

Tanaka and Kudo (2003) have shown that the noise component of the projection accessed at the qth order will appear in the final image of the complete cycle of the sub-iterations with a propagation efficiency given by

$$\varepsilon(q) = \lambda(q) \prod_{r=q+1}^{M-1} \left(1 - \lambda(r) \left\langle g^2(\phi) \right\rangle_\phi \right) \tag{2}$$

$$\left\langle g^2(\phi) \right\rangle_\phi = \frac{1}{M-1} \sum_{m=1}^{M-1} g^2(\phi) \qquad \text{with} \quad \phi = \pi m / M \tag{3}$$

where $g(\phi)$ is the geometrical correlation coefficient (GCC) of two LORs, ϕ is the angle between the two LORs, and $\left\langle \bullet \right\rangle_\phi$ denotes a constant obtained by averaging with respect to ϕ. Denoting the two LORs by LOR-1 and LOR-2, the GCC is defined by

$$g(\phi) = \sum_{j=1}^{J} a_{1j} a_{2j} \Bigg/ \left(\sum_{j=1}^{J} a_{1j}^2 \sum_{j=1}^{J} a_{2j}^2 \right)^{1/2} \tag{4}$$

where a_{1j} or a_{2j} is the probability that a photon emission from pixel j is recorded in the LOR-1 or LOR-2, respectively. If we define the relaxation parameter $\lambda(q)$ by

$$\lambda(q) = \beta_0 / (\beta_0 + q) \tag{5}$$

$$\beta_0 = \left\langle g^2(\phi) \right\rangle_\phi^{-1} \tag{6}$$

we can show that the noise propagation efficiency is independent of q. That is, we have, from equations (2), (5) and (6), $\varepsilon(q) = \beta_0 / (\beta_0 + M - 1) = $ constant. DRAMA-2D with the relaxation parameter defined by equation (5) will then provide uniform noise propagation.

(a) 2D-PET model   (b) 3D-PET model
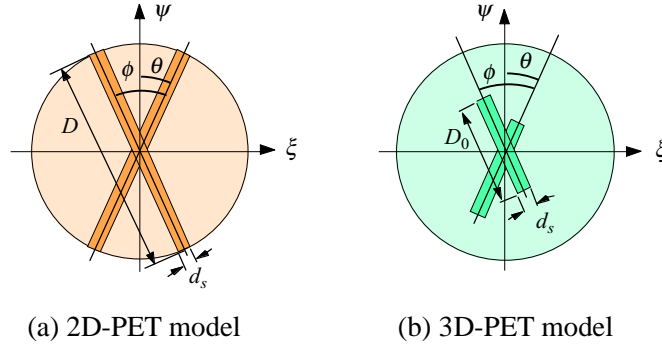
Figure 1. Two LORs model for calculating geometrical correlation coefficient.

In practice, we consider two LORs crossing at angle ϕ ($\leq \pi/2$) and calculate $g(\phi)$ assuming that the LORs have a Gaussian cross-section corresponding to the post-smoothing (see figure 1(a)). The GCC between the two LORs is given by (Tanaka and Kudo 2003)

$$g(\phi) = \frac{2}{D \cos \theta} \int_0^{D/2} \exp \left\{ -\frac{(\psi \sin \theta)^2}{\sigma_s^2} \right\} d\psi \tag{7}$$

where $\theta = \phi/2$, σ_s is the standard deviation of the Gaussian post-smoothing and D is the diameter of the field of view to be reconstructed. Using equation (7) in equations (3), (5) and (6), we can calculate β_0

and $\lambda(q)$.   However, the $\lambda(q)$-value thus obtained is a function of M, even though there is no reason that $\lambda(q)$ depends on M.   In the present paper, we describe a new simple expression of β_0 in the followings. The new expression of β_0 does not include the calculation of the GCC, and the obtained β_0-value (and $\lambda(q)$-value too) is independent of M.   The implementation of DRAMA becomes quite simple with this new expression of β_0.

We consider the minimum angular interval $\Delta\phi$ to be considered to compute the average geometrical correlation $\left\langle g^2(\phi) \right\rangle_\phi$ in equation (3).   Usually M is set to a sufficiently large number than that necessary to yield required spatial resolution, and the angular interval is equal to π/M (in 2D-PET model).   In the iterative image reconstruction with post-smoothing, the effective number of views is reduced to a value defined by the consistency condition (Natterer 1986) on the relation between the spatial resolution d_s and the minimum necessary number of angular views n_ϕ (in π), which is derived from Shannon's sampling theorem.   The relation is given by $n_\phi = \pi D/(2d_s)$, where d_s is the smoothing width[1] of the post-smoothing.   The smoothing width of the Gaussian post-smoothing is $d_s = 2\sqrt{\pi}\sigma_s$.   The angular interval in the consistency condition is then given by

$$\Delta\phi = \pi/n_\phi = 2d_s/D . \tag{8}$$

Considering the effect of the post-smoothing, it is reasonable to define β_0 using the angular interval given by equation (8).   For $\phi \geq \Delta\phi$, the value of the integrand of equation (7) at the upper limit of the integration, $\psi = D/2$, is negligibly small ($\leq \exp(-\pi)$), and then we can execute the integration by replacing the upper limit of the integral with infinity.   The result is

$$g(\phi) \approx 2\sqrt{\pi}\sigma_s/(D\sin\phi) = d_s/(D\sin\phi) . \tag{9}$$

We assume that the summation in equation (3) is approximated by the integral with the lower limit of $\Delta\phi$. Then we have

$$\beta_0 \approx \left(2\int_{\Delta\phi}^{\pi/2} g^2(\phi)\,d\phi \right)^{-1} = \frac{\tan\Delta\phi}{2} \frac{D^2}{d_s^2} \approx \frac{\Delta\phi}{2} \frac{D^2}{d_s^2} . \tag{10}$$

Using equation (8) in equation (10), we have a simple expression of β_0 as

$$\beta_0 \approx D/d_s . \tag{11}$$

We confirmed that the β_0-value obtained with the integration (equations (10) and (11)) is 5~6% larger than the value obtained with the summation (equation (3)) with $M=n_\phi$ for d_s=1.5~6.0 pixels and D=128~256 pixels.   The difference is allowable.

It is worth noting that the ratio D/d_s ($= \beta_0$) corresponds to the ratio of the information content on positioning of a resolution element having size $d_s \times d_s$ to that of an LOR having width d_s and length D. We call the ratio "CT-loss", because it reflects the ratio of the noise variance of a 2D-PET image to that of a gamma camera image obtained with the same total counts.   In other words, 2D-PET imaging needs larger total counts than gamma camera imaging by a factor of about $\beta_0 \approx D/d_s$ to obtain the similar image quality (Tanaka and Iinuma 1976).

---

[1] The smoothing width d_s of a filter function $f(x)$ (≥ 0) is defined as the width of the rectangular filter having the same smoothing effect as that of the filter $f(x)$ for Poisson noise:

$$d_s = \left(\int_{-\infty}^{+\infty} f(x)\,dx \right)^2 \Big/ \int_{-\infty}^{+\infty} f^2(x)\,dx .$$

2.2. DRAMA-3D

2.2.1. Geometry and model of 3D-PET. We consider a multi-ring 3D-PET model as shown in figure 2. We denote the diameter of the detector ring by D_{ring}, the diameter of the reconstructed field of view by D, and the detector ring pitch by d_{pitch}. We consider to reconstruct a number of contiguous slices, and we assume that the slice thickness w is equal to a half of the detector ring pitch, i.e. $w = d_{pitch}/2$. The slices are divided into direct-slices or cross-slices. Consider an oblique LOR with a ring difference δ. The slant angle Θ is given by $\tan\Theta = \delta d_{pitch}/D_{ring}$. In the conventional PET scanner, the finite axial length of the detector ring limits the maximum ring difference δ_{max}. As a result, the value of δ_{max} varies not only along different slices (smallest in the end-slices and largest in the central slice) but also changes with the distance from the axis of the detector ring. These situations are inconvenient to develop the theory of DRAMA-3D. We then assume that δ_{max} is determined by a given constant value and is not affected by the detector rings, in developing the theory on DRAMA-3D (section 2). We also perform simulation studies (section 3) to check the validity of DRAMA-3D under the same assumption (constant δ_{max}). However, we have to check carefully the effect of the assumption. We will report the results of the simulation study with a PET scanner having a limited axial length in section 3.6. Note that, in some kinds of PET systems, approximately flat axial-profile of δ_{max} is obtained by stepwise or continuous scanning of the patient bed or the detector gantry in the axial direction.
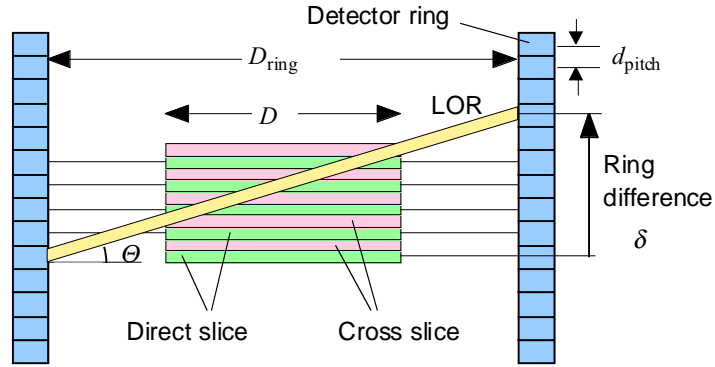
Figure 2. Configuration of a 3D-PET scanner.

2.2.2. Reconstruction algorithm. We assume again that coincidence data are obtained along *I* lines of response (LORs) and denote by y_i ($1 \leq i \leq I$) the number of detected coincidence events along the *i*th LOR. These data are grouped (subsetized) by the azimuthal angle ϕ and the ring difference δ (0, 1, $\cdots$, δ_{max}), where δ_{max} is the maximum ring difference. The range of the azimuthal angle ϕ is 0~π for δ=0 and 0~2π for δ>0. Each subset consists of parallel LORs having constant δ and ϕ. We consider a square image matrix of $N\times N$ boxels on each slice, and photon emission from boxel *j* is denoted by x_j ($1 \leq j \leq J$). In the 3D-PET, we usually have a sufficiently large number of views (projections), and then we consider here single main iteration (one-pass reconstruction) and drop the index *k* of the main iteration for simplicity. The update equations of the proposed DRAMA-3D are

$$r = 0. \tag{12}$$
For $n = 0, 1, \cdots, \delta_{max}$ {
    For $q = 0, 1, \cdots, q_{max}(\delta) - 1$ {

$$x_j^{(n,q+1)} = x_j^{(n,q)} + \lambda(\delta,r)\frac{x_j^{(n,q)}}{C_j}\sum_{i \in S_{n,q}} a_{ij}\left(\frac{y_i}{\sum_{j'=1}^{J} a_{ij'}\, x_{j'}^{(n,q)}} - 1\right) \tag{13.1}$$

$$x_j^{(n+1,0)} = x_j^{(n,M)} \tag{13.2}$$

$$C_j = \max_{n,q}\sum_{i \in S_{n,q}} a_{ij} \tag{13.3}$$

$$r \mathrel{+}= 1 \tag{13.4}$$

     }

   }

where n is the index of the access order of the ring difference $\delta(\geq 0)$, q is the index of the access order of azimuthal angle ϕ and $q_{max}(\delta)$ is the number of the azimuthal angles of a subset having ring difference δ. That is, $\delta=\delta(n)$, $\phi=\phi(q)$, $q_{max}(0)=M$ and $q_{max}(\delta>0)=2M$. $S_{n,q}$ is the subset of LORs having the same azimuthal angle ϕ and ring difference δ. $\lambda(\delta, r)$ is the relaxation parameter $(0 < \lambda(\delta, r) \leq 1)$ and r is the index of the overall access order of a subset. The value of r is initialized by equation (12) prior to the iteration, and is incremented with 1 inside the q-loop by equation (13.4). The other parameters are same as those used in section 2.1.

2.2.3. Reciprocal of mean squared GCC: $\beta(\delta)$. In DRAMA-2D, the parameter β_0 plays an important role in defining the optimal relaxation parameter (see equation (5)). β_0 is the reciprocal of the mean squared GCC between two LORs (see equation (6)). In DRAMA-3D, we suppose two oblique LORs having the same ring difference δ intersect an imaging slice, and we define $g(\delta,\phi)$ as the GCC between the two LORs on the slice, where ϕ $(0 \leq \phi \leq \pi)$ is the azimuthal angle between the two LORs (see figure 1(b)). It is reasonable to consider that $\beta(\delta)$ defined by the following equations (14) plays the similar role to β_0 in DRAMA-2D.

$$\beta(\delta) = \left\langle g^2(\delta,\phi)\right\rangle_\phi^{-1} \qquad\qquad \delta > 1 \tag{14.1}$$

$$\beta(\delta) = \beta_0 \qquad\qquad \delta = 0, 1 \tag{14.2}$$

where $\left\langle \bullet \right\rangle_\phi$ denotes a constant obtained by averaging with respect to ϕ. The GCC between the two LORs in the 2D-PET model is given as equation (A.7) in the previous paper (Tanaka and Kudo 2003). However, in the case of 3D, we have to modify it by including the effect of the intersection between the oblique LORs and a slice of interest.

   It is known that oblique projections lack low (and zero) frequency components of the 2D-image of the slice, and the frequency distribution depends on the profile of the intersection between the LOR and the slice (Tanaka and Amo 1998) (see Appendix A). We then consider the profile of the intersection for our PET model. In general, the axial profile of the LOR depends on the detector response and the distances from the detectors. However, we assume here a very simple model. That is, we assume the axial thickness of the LOR is equal to the slice thickness w $(=d_{pitch}/2)$ and the axial response is rectangular. The profile of the intersection is then expressed as an isosceles triangle having the base length of $2L$ as shown in figure 3. Letting Θ be the slant angle, we have $L = w/\tan\Theta$. The triangular profile is approximated by a Gaussian profile having the same smoothing width as that of the triangle, $D_0=3L/2$, for the convenience for the following calculation. The standard deviation of the Gaussian profile is $\sigma_0 = 3L/(4\sqrt{\pi})$. The GCC between the two oblique LORs crossing with azimuthal angle ϕ (see figure 1(b)) is then given by equation (B.2) in Appendix B, but the equation is too complicated for the following analysis. We then made further approximation to obtain a simpler expression given by (see Appendix B)

$$g(\delta,\phi) = c \int_{-\infty}^{+\infty} \int_{-\infty}^{+\infty} \exp\left\{-\frac{(\xi_\theta - \xi)^2 + (\xi_\theta + \xi)^2}{2\sigma_\theta^2}\right\} \exp\left(-\frac{\xi^2 + \psi^2}{4\sigma_0^2}\right) d\xi\, d\psi \tag{15}$$

where $\theta = \phi/2$, $\xi_\theta = \psi \tan\theta$, $\sigma_\theta = \sigma_s/\cos\theta$, and c is the normalizing constant. Equation (15) has two exponential terms. The second exponential term was newly introduced for the 3D-PET model to adapt to the finite length of the intersections. From equations (15) and (14.1), we have (see Appendix C)

$$\beta(\delta) = \sqrt{\sigma_0^2 + \sigma_s^2}\big/\sigma_s = \sqrt{D_0^2 + d_s^2}\big/d_s \qquad \delta > 1 \tag{16.1}$$
$$D_0 = 2\sqrt{\pi}\sigma_0 = 3L/2 \tag{16.2}$$

where D_0 is the smoothing width of the triangular profile of the intersection between the oblique LORs and the slice of interest. In the above calculation, we have neglected the truncation of the triangular intersection due to the limited field of view of the slice. In practice, it is apparent that $\sqrt{D_0^2 + d_s^2}$ should not be larger than the diameter of the field of view, D, and hence we have

$$\beta(\delta) = \min\left(\frac{\sqrt{D_0^2 + d_s^2}}{d_s}, \frac{D}{d_s}\right) \tag{17}$$
$$\approx \min\left(\frac{D_0}{d_s}, \frac{D}{d_s}\right) \qquad \text{when } d_s \ll D_0. \tag{18}$$

Note that $\beta(\delta)$ is given by the similar expression to β_0 in equation (11), and that its value corresponds to the CT-loss D_0/d_s in the 3D-reconstruction.
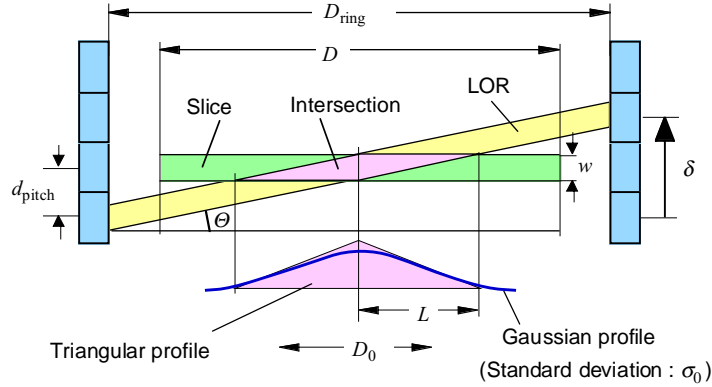
Figure 3. Profiles of the intersection of an LOR and a slice.

2.2.4. Noise propagation efficiency $\varepsilon(\delta, r)$ and optimal relaxation parameter $\lambda(\delta, r)$. Suppose a subset having the ring difference δ is accessed at the order r, and consider the propagation efficiency $\varepsilon(\delta, r)$ of the noise contained in the subset to the end of each main iteration. Up to a reasonable approximation, the noise propagation efficiency is expressed in the similar manner to the case of DRAMA-2D (see equations (2) and (14.1))

$$\varepsilon(\delta,r) = \lambda(\delta,r) \prod_{s=r+1}^{r_{\text{out}}} \left(1 - \lambda(\delta_s,s)\left\langle g^2(\delta_s,\phi)\right\rangle_\phi\right) \tag{19.1}$$

$$= \lambda(\delta,r) \prod_{s=r+1}^{r_{\text{out}}} \left(1 - \frac{\lambda(\delta_s,s)}{\beta(\delta_s)} \right) \tag{19.2}$$

where r_{out} is the last access order and δ_s is the ring difference of the subset accessed at the order s. $\lambda(\delta_s,s)/\beta(\delta_s)$ in equation (19.2) implies the rate of the image density deposited by the sth subset, and the noise component of the old image is erased by this rate. The factor in the parentheses in equation (19.2) represents the survival rate of the noise component before accessing the sth subset.

In DRAMA-2D, it was shown that the relaxation parameter given by equation (5) provides uniform noise propagation in section 2.1. In DRAMA-3D, we can show that the following $\lambda(\delta, r)$ provides uniform noise propagation

$$\lambda(\delta,r) = \frac{\beta(\delta)}{\alpha\beta_0 + r} \tag{20}$$

where β_0 and $\beta(\delta)$ are defined by equations (11) and (17), respectively, r is the access order of a subset, and α (≥ 1) is the damping factor to stabilize excessive updating at the early stage of iterations with small r. Using equation (20) in equation (19.2), we have

$$\varepsilon(\delta,r) = \frac{\beta(\delta)}{\alpha\beta_0 + r} \prod_{s=r+1}^{r_{\text{out}}} \frac{\alpha\beta_0 + s - 1}{\alpha\beta_0 + s} = \left(\frac{\beta(\delta)}{\alpha\beta_0 + r} \right) \left(\frac{\alpha\beta_0 + r}{\alpha\beta_0 + r_{\text{out}}} \right) \tag{21.1}$$

$$= \frac{\beta(\delta)}{\alpha\beta_0 + r_{\text{out}}}. \tag{21.2}$$

The first factor of equation (21.1) represents the intensity of the input noise, and the second factor quantifies the decrease of the noise by the following iterations. Equation (19.2) implies that, up to a reasonable approximation, the magnitude of the input noise depends on δ, but the decrease of the noise is independent of the ring difference δ_s of the following iterations. In other words, equation (21.2) is valid even if the following iterations are performed with subsets having ring differences different from δ. Thus, the above theory can be applied in any mode of data access described in the following section 2.2.5. It is interesting to note that $\varepsilon(\delta,r) = \lambda(\delta, r_{\text{out}})$.

The intuitive understanding of $\varepsilon(\delta, r)$ is as follows. Equation (21.2) can be rewritten as a product of two factors

$$\varepsilon(\delta,r) = \left(\frac{\beta(\delta)}{\beta_0} \right) \left(\frac{\beta_0}{\alpha\beta_0 + r_{\text{out}}} \right) \approx \left(\frac{D_0}{D} \right) \left(\frac{\beta_0}{\alpha\beta_0 + r_{\text{out}}} \right) \qquad \delta > 1. \tag{22}$$

The first factor, D_0/D, is equal to the reciprocal of the effective number of slices, which cross an oblique LOR having ring difference δ. The oblique LOR contains the information (and noise) of all these slices, and hence a fraction D_0/D of the total information of the LOR should be allocated to each slice. $\beta(\delta)/\beta_0$ or D_0/D is the allocation factor. The second factor represents noise propagation corresponding to $\varepsilon(q)$ in DRAMA-2D. The above allocation is rather approximate, because the distribution of activity along the LOR is not generally uniform. The ambiguity of the allocation may cause unstable updating when r is small and δ is large. The instability will be relaxed by using $\alpha > 1$ in equation (20) as shown later in section 3.2.

It is reasonable that $\beta(\delta)$ is involved in $\lambda(\delta, r)$ and $\varepsilon(\delta, r)$, from the concept of the CT-loss. That is, since the variance of noise deposited to the slice is inversely proportional to the CT-loss $D_0/d_s \approx \beta(\delta)$, the input rate of the data should be proportional to $\beta(\delta)$ in order to equalize the noise variance for various

oblique projections having different ring differences. $\lambda(\delta, r)$ given by equation (20) will then provide uniform noise propagation regardless of any choice of access order of δ. The rationality of the δ-dependence of $\lambda(\delta, r)$ will be confirmed by the simulation studies described in section 3.

2.2.5. Modes of data access. Performance of DRAMA-3D depends on the access order of the ring difference δ as shown later (see section 3.2). We consider the following four modes of data access in order to understand the effect of access order of δ

  (a) *Ascending* mode in which $\delta(n) = n$.

  (b) *Descending* mode in which $\delta(n) = \delta_{max} - n$.

  (c) *Constant increment scheme* (*CIS*) mode based on the recursive formula: $\delta(n) = (\delta(n-1) + \text{constant}) \text{ Mod } (\delta_{max} + 1)$. If $\delta(n)$ is already used, add one until obtaining a new value. We use the integer nearest to $0.7\delta_{max}$ as the constant.

  (d) *Random mode* in which we choose δ and ϕ randomly and independently of n and q.

In (a), (b) and (c), δ is first selected and the data for all azimuthal angles are processed according to the selected access order, q. After all azimuthal angles are processed, the next δ is selected.

3. Simulation studies

3.1. General descriptions

We consider a multi-ring 3D-PET scanner as shown in figure 2. The detector ring diameter D_{ring} is 80 cm, the axial detector ring pitch d_{pitch} is 8 mm, and the slice thickness w is 4 mm (= a half of the detector pitch). The size of the reconstructed image matrix is 128×128 for each slice, the boxel size is $4 \times 4 \times 4$ mm^3, and the number of azimuthal angles is 256 in 2π for $\delta > 0$. We performed simulation studies using computer generated projection data of mathematical phantoms. We controlled the transaxial spatial resolution of reconstructed images by transaxial post-smoothing with a Gaussian filter having full-width at half maximum (FWHM) of 2 pixels (8 mm). We can apply axial post-smoothing (section 3.5), but we did not apply any axial smoothing unless otherwise stated. The values of $\beta(\delta)$ with the above condition are plotted in figure 4.
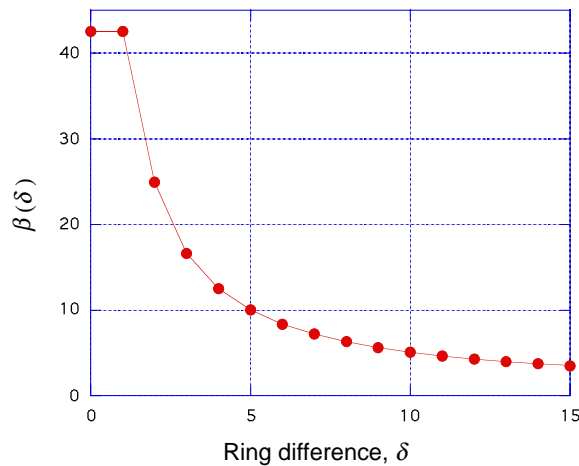
Figure 4. Examples of $\beta(\delta)$ (δ_{max}=15).

9

We evaluated the performances of the algorithms by the following four items. In these tests, we reconstructed the images of a number of contiguous slices, assuming that the axial length of the detector is sufficiently long. The axial length of the phantom is equal to the axial length of the contiguous slices. We performed the following tests for the two adjacent slices (one is a direct-slice and the other is a cross-slice) axially located at the middle of the reconstructed slices, and we reported the mean value of the two test results. The number of reconstructed slices was $(\delta_{max}+1)/2$. For an example, when δ_{max} =15, we reconstructed 8 slices (sl-1, sl-2, $\cdots$, sl-8), and the mean value of the test results for sl-4 and sl-5 was reported. We confirmed that the further increase of the number of the reconstructed slices did not bring meaningful difference in the results. For the tests with noisy data, we assumed that the total counts of the projections with $\delta = 0$ is 2×10^5 per slice.

- *Structural error* (%): This item measures how the reconstructed image is close to the phantom image. The *structural error* was calculated by taking the average of the absolute difference between the reconstructed boxel value and the phantom value over the whole region of interest, and expressed it as the ratio to the mean density of the phantom[2]. For this test, we used the phantom consisting of a cylindrical uniform phantom (40 cmφ), a cylindrical hot area (16 cmφ), a cold area (16 cmφ) and a rod source (1 cmφ). The phantom was uniform axially. We smoothed the phantom with the same filter as that used in the post-smoothing for the reconstructed image. Statistical noise was not added in this test. An example of the reconstructed image of a slice is shown in figure 5(a).

- *Spatial resolution* (transverse, pixels): We assumed a phantom consisting of a cylindrical uniform phantom (40 cmφ) and a rectangular plane source (4 mm thickness) embedded on the cylindrical phantom. The plane source was placed in parallel to the axis in such a way that the phantom was uniform axially. We defined transverse *spatial resolution* as the FWHM of the spread function of the reconstructed image of the plane source evaluated by fitting it with a Gaussian function. The value was expressed in terms of pixels. An example of the reconstructed image of a slice is shown in figure 5(b).

- *RMS noise* (%): Root mean square (RMS) noise of the reconstructed image was evaluated with a uniform cylindrical phantom (see figure 5(c)). The value was calculated by taking the average of the squared difference between the reconstructed boxel value and the phantom value over the central circular region having 80% of the phantom in diameter[3].

- *Noise propagation ratio* (NPR): We defined *NPR* in order to check the uniformity of the noise propagation. *NPR* is defined as the ratio of *RMS noise* of the reconstructed image with noise on data having $\delta > \delta_{max}/2$ (data of $\delta < \delta_{max}/2$ are noiseless) to that with noise on data having $\delta < \delta_{max}/2$ (data of $\delta > \delta_{max}/2$ are noiseless). Both the images were reconstructed using all ring difference, $0 \le \delta \le \delta_{max}$. More precisely, *NPR* is defined by

$$NPR = \frac{RMS\ noise \text{ of the image with noise on } \delta > \delta_{max}/2}{RMS\ noise \text{ of the image with noise on } \delta < \delta_{max}/2} \left(\frac{\delta_{max}}{\delta_{max}+1} \right). \tag{23}$$

The factor in the parentheses is the correction factor to the fact that number of the azimuthal angles of δ =0 is a half of that of δ >0. *NPR* ≈ 1 indicates uniform noise propagation, and *NPR* > 1 implies that the noise of larger δ contributes more strongly to the final image than that of smaller δ.

---

[2] We evaluate the *structural error* using L_1 norm in a region larger than the phantom. If we evaluate using L_2 norm, the error at the edge of the phantom appears more strongly than the error at the flat portion of the phantom, and hence it is better to evaluate using L_1 norm.

[3] We evaluate the *RMS noise* using L_2 norm in a flat-area smaller than the phantom. If we evaluate in the area larger than (or equal to) the phantom, the estimated *RMS noise* will be affected by the structural recovery.

(a) Structural error   (b) Spatial resolution   (c) RMS noise
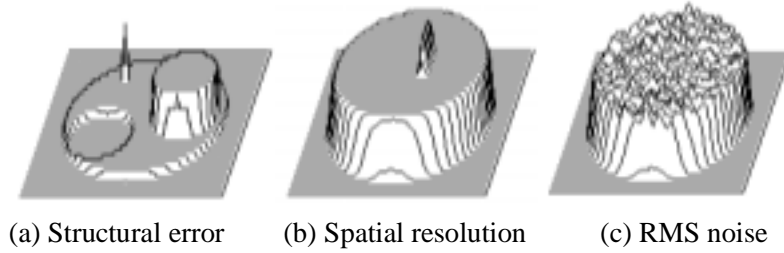
Figure 5. Examples of images reconstructed in the performance tests.

3.2. Modes of data access and damping factor

Performances of DRAMA-3D depend on the mode of data access (see section *2.2.5.*) and the damping factor α in equation (20). We determined the α-value in such a way that the performance is stable with all modes of data access. Figure 6 shows the plots of RMS noise versus structural error with various damping factor α. The maximum ring difference is $\delta_{max} = 15$. With $\alpha = 1$, the RMS noise of the descending mode and CIS mode is excessively high. The reason for this is that the data of large δ are accessed at early stage (small r) and the iteration becomes unstable (see the second paragraph from the end in section 2.2.4). The excessive noise is effectively reduced by using $\alpha \geq 2$. Figure 7 shows the noise propagation ratio (*NPR*) for various δ_{max} with $\alpha = 1$ (left) and $\alpha = 3$ (right). It is seen that the excessively large *NPR*s in the descending mode and CIS mode are reduced to normal values around unity by using $\alpha = 3$. Although the ascending mode is quite stable even with $\alpha = 1$, we have used $\alpha = 3$ for all access modes in the following studies.

Figure 8 shows (a) the plots of $\lambda(\delta, r)$ ($q = 0$) as a function of access order n and (b) its trajectories for various access modes. In the ascending mode, the data with $\delta = 0$ and $\delta = 1$ are concerned with only direct-slices and cross-slices, respectively, and these slices are independent of each other. Then, $\lambda(\delta, r)$ given by equation (20) was modified in such a way that $\lambda(1, r) = \lambda(0, r)$ holds by redefining it

$$\lambda(\delta, r) = \frac{\beta(\delta)}{\alpha \beta_0 + q + \max(0, n-1)2M} \qquad \text{(in ascending mode).} \qquad (24)$$

In the random mode, the value of $\lambda(\delta, r)$ appears randomly in the region between the two curves marked with "random+" and "random–" in figure 8(b).
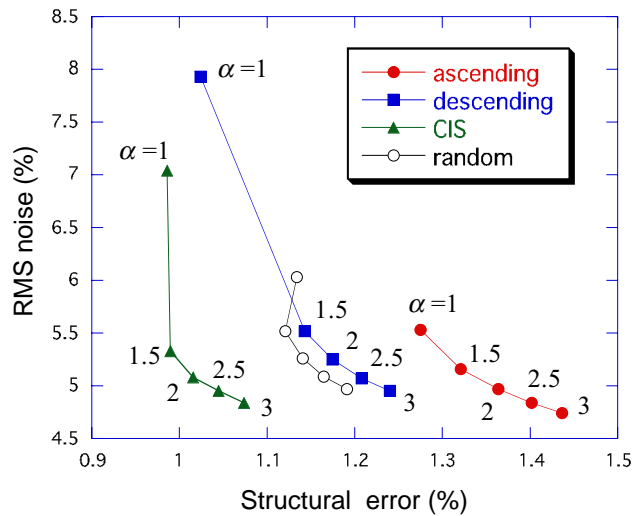
Figure 6. Effect of damping factor α on the plots of RMS noise versus structural error ($\delta_{max} = 15$).

11
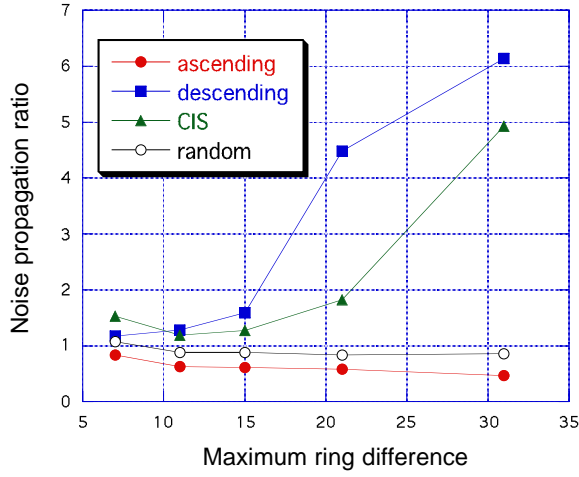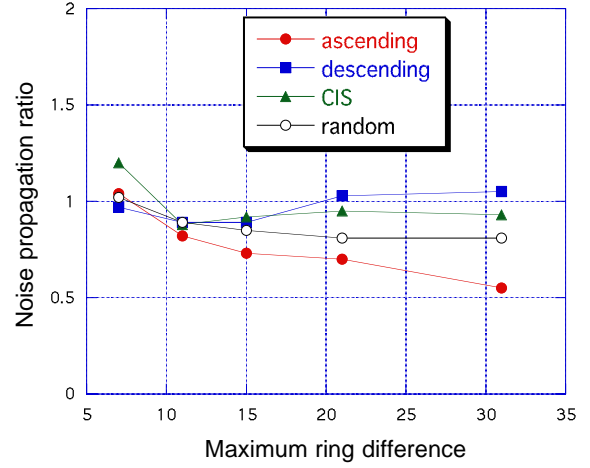
(a) $\alpha = 1$ (b) $\alpha = 3$

Figure 7. Effect of damping factor α on the plots of noise propagation ratio (*NPR*) versus δ_{max}.
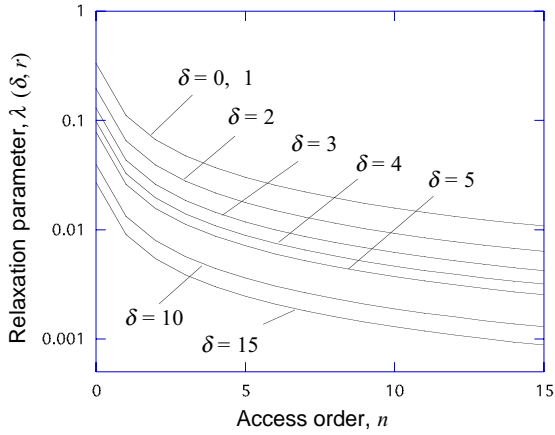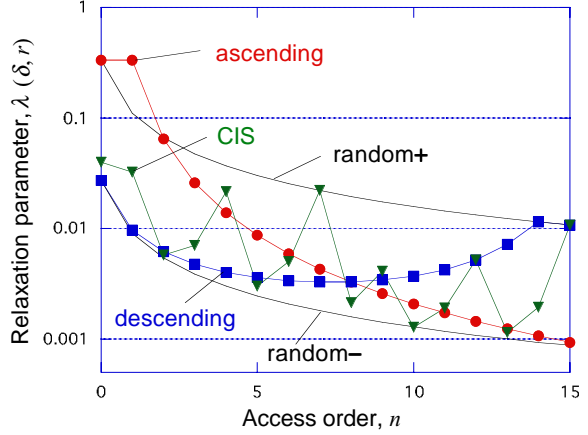
(a) Relaxation parameters   (b) Trajectories of various modes

Figure 8. Relaxation parameters and their trajectories for various access modes ($\delta_{max} = 15$).

3.3. Performance of DRAMA-3D

Figure 9 shows the performances of DRAMA-3D as a function of the access order n. These figures demonstrate how the images are formed in a single iteration for the four modes of data access. The maximum ring difference δ_{max} is 15. It is seen that the RMS noise is similar for all the modes of data access. This is a consequence of the adequate δ-dependence of $\lambda(\delta, r)$. The value on spatial resolution approaches to the final value asymptotically (the resolution of the post smoothing is 2 pixels in FWHM) for all the modes of data access, but the convergence of the ascending mode is a bit slower than the others. The reason for this may be the rapid decrease of $\lambda(\delta, r)$ with n in the ascending mode (see figure 8(b)).

12

As described before, oblique projections lack low (and zero) frequency components of the transaxial image (Tanaka and Amo 1998) (see Appendix A). For this reason, we hypothesize that the low frequency components are not properly reconstructed in the late stage of iteration of the ascending mode, and it may cause a little larger structural error in the late stage of the ascending mode (figure 9(a)). In the descending mode, on the other hand, updating of low frequency components is not properly performed in the early stage of iteration, and it results in the abnormal behavior on the spatial resolution (figure 9(b)) and a bit larger structural error at the early stage of iteration (figure 9(a)). The CIS mode and the random mode show similar performances to each other, and both the modes provide better performances for structural accuracy than the other modes. This will be by virtue of the balanced updating for all frequency components. We recommend the use of either of these two modes. The results of the one-pass reconstruction with various δ_{max} are summarized in table 1.

(a) Structural error

(b) Transaxial spatial resolution

(c) RMS noise
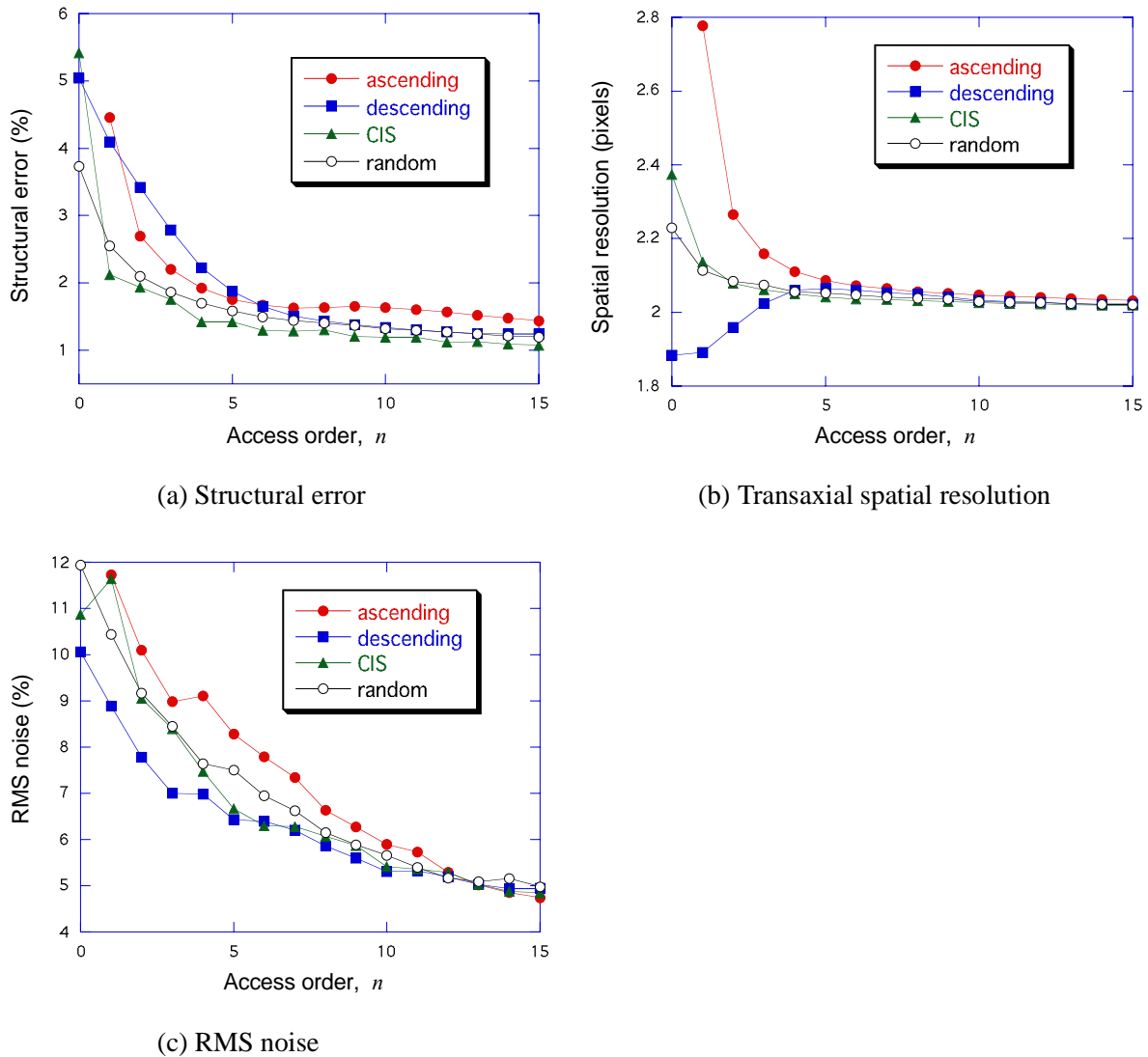
Figure 9. Performances of DRAMA-3D (δ_{max}=15).

Table 1. Performances of DRAMA-3D (one-pass reconstruction)

Test item	Mode of access	$\delta_{max}=11$	$\delta_{max}=15$	$\delta_{max}=21$	$\delta_{max}=31$
Structural Error (%)	Ascending	1.501	1.437	1.328	1.212
	Descending	1.325	1.240	1.156	1.031
	CIS	1.125	1.074	1.040	0.931
	Random	1.203	1.191	1.104	0.991
Resolution (FWHM, pixels)	Ascending	2.037	2.032	2.027	2.022
	Descending	2.020	2.022	2.013	2.014
	CIS	2.026	2.020	2.019	2.015
	Random	2.023	2.021	2.017	2.008
RMS noise (%)	Ascending	5.60	4.74	4.54	4.15
	Descending	5.70	4.95	4.38	3.40
	CIS	5.52	4.84	4.22	3.62
	Random	5.54	4.97	4.48	3.77

3.4. Comparison with related algorithms, DRAMA(β) and RAMLA(λ)

We have performed comparative studies on the performances of DRAMA-3D with two related algorithms. The first algorithm is a simplified version of DRAMA-3D having a relaxation parameter $\lambda(r) = \beta/(\alpha\beta_0 + r)$ where β is a constant. We named the algorithm as "DRAMA(β)". The purpose of DRAMA(β) is two-fold. The one is to check the effect of discarding $\beta(\delta)$ in $\lambda(\delta, r)$ and the other is to reveal the difference in behavior between DRAMA(β) and DRAMA-3D. The second algorithm is "RAMLA(λ)", in which the relaxation parameter λ is a subset-independent constant. Since there is no simple way to determine the suitable values of β and λ, we determined them manually by trial and error. We used $\alpha = 3$ in DRAMA(β) too. The maximum ring difference δ_{max} is 15.

Figure 10 shows the plots of RMS noise versus structural error for the four modes of data access. It is shown that, in the ascending mode, the data points of RAMLA(λ) are very far from those of DRAMA-3D, which implies that RAMLA(λ) is useless in this mode. The reason for this is that the ascending mode requires a rapidly decreasing λ-value with *n* as shown in figure 8(b) while the λ-value is constant in RAMLA(λ). On the other hand, in the descending mode, RAMLA(λ) behaves almost similarly to DRAMA-3D with a suitable λ-value. This may be due to the fact that the trajectories of $\lambda(\delta, r)$ of the descending mode is U-shaped (see figure 8(b)), which is roughly approximated by the constant λ in RAMLA(λ). Note that DRAMA(β) is reasonably good in any mode. In particular, in the random mode and CIS mode, DRAMA(β) provides the much closer performances to DRAMA-3D than RAMLA(λ). We compared the RMS noise of the three algorithms at the same structural error for the random mode of data access. The results are summarized in table 2. The values in parentheses are the ratio to the RMS noise of DRAMA-3D. Note that the RMS noise of RAMLA(λ) is larger than those of DRAMA-3D by a factor of about 1.24~1.33, but the difference of noise between DRAMA(β) and DRAMA-3D is not so large (4~11%). The noise propagation ratio, *NPR*, is around 2.0 in both the algorithms, which implies that noise of the data of larger δ affects more to the result than the data of smaller δ. On the other hand, *NPR* of DRAMA-3D is close to unity (0.81~0.89), which implies that the δ-dependence of $\lambda(\delta, r)$ is reasonable.
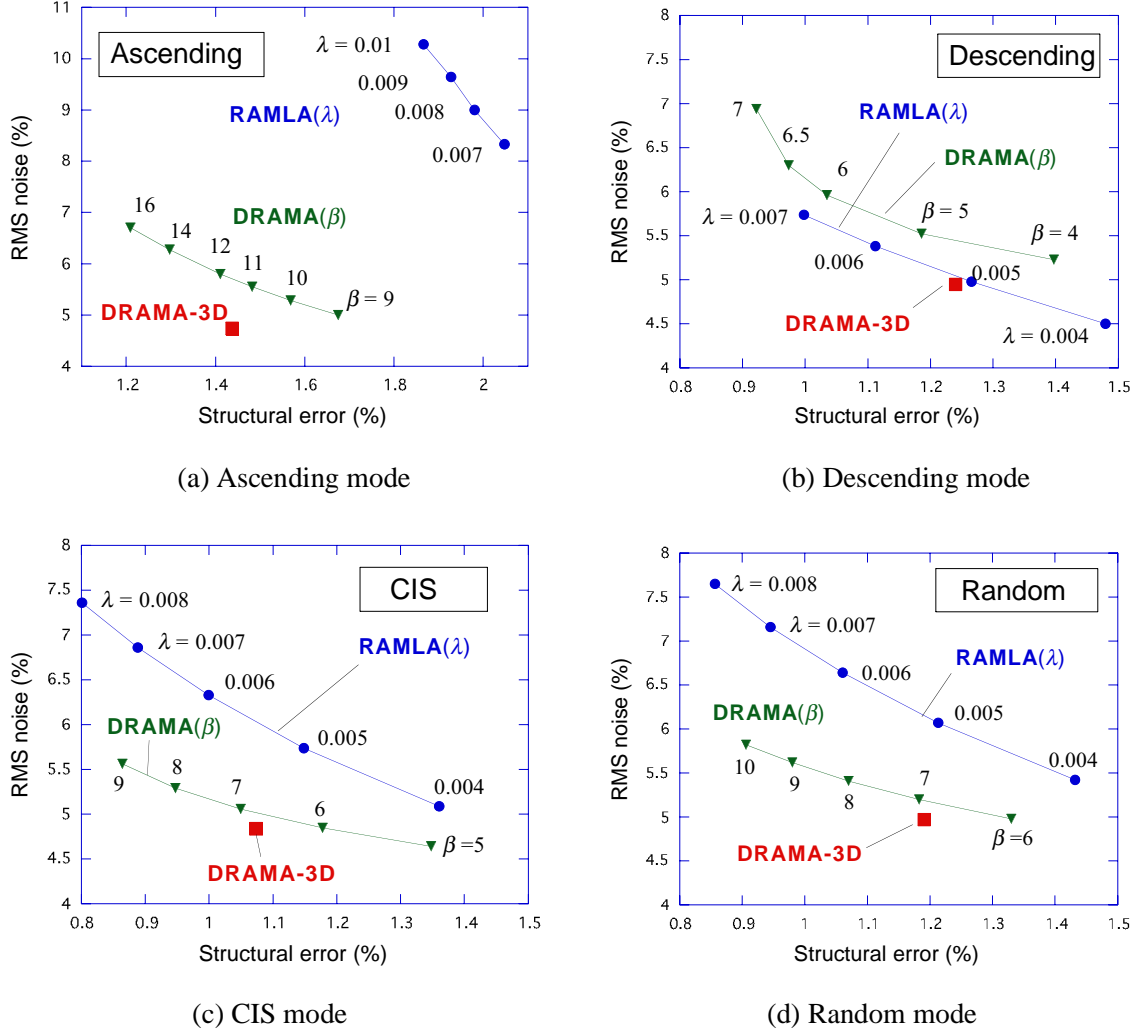
Figure 10. Plots of RMS noise versus structural error of the three algorithms for the four data access modes. (δ_{max}=15).

Table 2. Comparison of DRAMA-3D, DRAMA(β) and RAMLA(λ) at the same structural error.

		δ_{max}=11	δ_{max}=15	δ_{max}=21	δ_{max}=31
DRAMA-3D	RMS noise (%)	5.54	4.97	4.48	3.77
	NPR	0.89	0.85	0.81	0.81
RAMLA(λ)	λ	0.0082	0.0051	0.0033	0.0019
	RMS noise (%)	6.95 (1.26)	6.15 (1.24)	5.64 (1.26)	5.02 (1.33)
	NPR	2.29	2.18	2.02	1.93
DRAMA(β)	β	8.8	7.0	5.3	4.7
	RMS noise (%)	5.74 (1.04)	5.20 (1.05)	4.73 (1.06)	4.20 (1.11)
	NPR	2.17	2.02	2.00	2.16

The values in parentheses are the ratio to the RMS noise of DRAMA-3D.　Data access is random mode.

3.5. Axial post-smoothing.

Although we have not applied axial smoothing so far, we can apply the axial post-smoothing in addition to the transaxial post-smoothing to reduce the statistical noise at the cost of the axial resolution.　We

have tested the effect of an axial filter having the relative weights (s_a:1:s_a) on the contiguous slices, where s_a ($0 \leq s_a \leq 1$) is a constant.   The phantom used in this test consists of 10 slices (slice-1, -2, …, -10). The slices-1, -4, -7 and -9 have different source distributions each other, and the rest slices are blank. The slices with even number are direct-slices and the others are cross-slices.   Figure 11 shows the reconstructed images with (a) s_a=0 (no axial smoothing) (b) s_a=0.25 and (c) s_a=0.50.   The transaxial post-smoothing filter was Gaussian having 2 pixels in FWHM, the maximum ring difference δ_{max} was 15 and the access order was the random mode (we confirmed that the other access modes yield similar results).   The images shown in figure 11(a) are quite similar to the phantom except the transaxial blur due to the transaxial smoothing.   It is seen that there is negligible axial cross-talk between slices when s_a=0 regardless of direct- or cross-slices, and that axial resolution is well recovered for finite values of s_a. This may not be surprising, because we did not take into account the axial response of the detector ring in this simulation, and we assume that the axial width of the LOR is sufficiently small.

   We have tested the effect of the axial post smoothing on statistical noise by repeating the RMS noise test (described in section 3.1) with various axial filters, and we found that the RMS noise is reduced by a factor of about 0.71 and 0.61 with the filter s_a=0.25 and s_a=0.50, respectively, as compared to the case of no axial smoothing (s_a=0).   These factors are very close to the theoretical values estimated by $\sqrt{1+2s_a^2}\big/(1+2s_a)$.
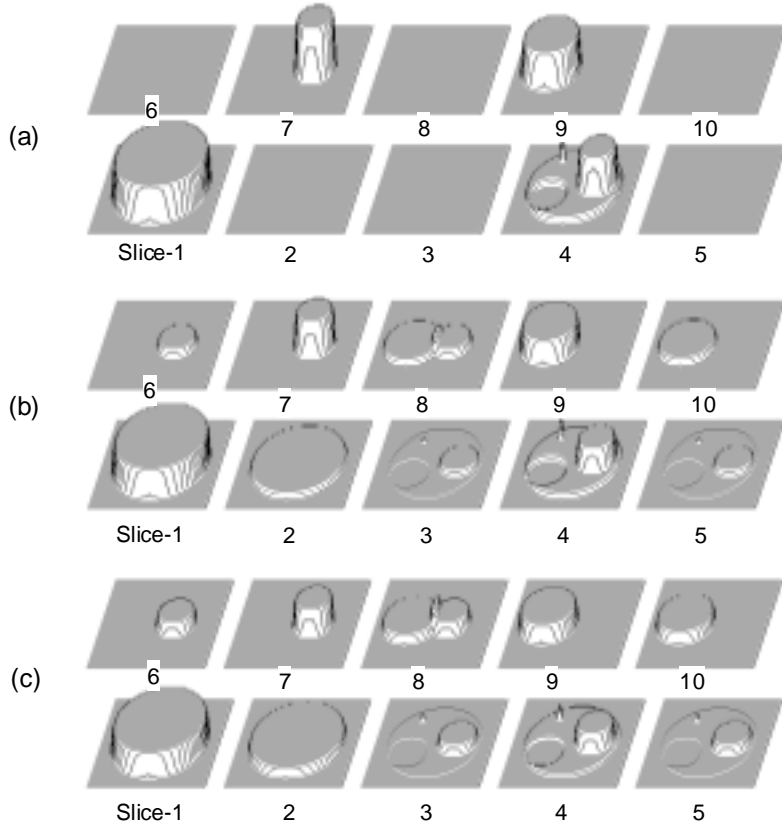
Figure 11. Images showing the effect of axial post-smoothing with a filter s_a : 1: s_a.
(a) $s_a = 0$, (b) $s_a = 0.25$ and (c) $s_a = 0.50$.

3.6. Performance of DRAMA-3D with a PET scanner having a limited axial length.

We have assumed that the maximum ring difference δ_{max} is constant in the theoretical treatment of DRAMA-3D (section 2.2.1).   We have also assumed a constant δ_{max} in the simulation studies described in section 3.1 ~ 3.5.   In a practical PET scanner, however, δ_{max} is usually determined by the limited axial

length of the detector ring. If all ring differences are accepted, δ_{max} (and sensitivity) vary along different slices, and the axial sensitivity is approximated by a triangular pattern. We have made simulation tests for the practical PET scanner assuming the number of detector rings was 12 and the number of slices was 23. Other parameters were same as those used so far. The maximum value of δ_{max} is 12 at the center of the central slices. The results are shown in figure 12 as the curves marked with "Limited ring". It is seen that the structural accuracy and the spatial resolution are highest at the central slices and degrade toward the end slices due to the varying sensitivity along different slices. The convergence is apparently insufficient at the slices near the ends due to the low sensitivity. We have also performed similar tests using a constant δ_{max} (=6) for comparison. The results are shown as the curves marked with "Constant δ_{max}" in the figure. It is seen that the structural accuracy and the spatial resolution are nearly uniform in the case of the constant δ_{max}. The above tests were performed with the random data access mode, but we have confirmed that similar results were obtained with the other data access modes. From these results, we expect that DRAMA-3D is feasible to apply to the practical PET scanner having a limited axial length, although further studies will be desirable on the details of the performance and on the limitation in applications.

(a) Structural error

(b) Transaxial spatial resolution

(c) RMS noise
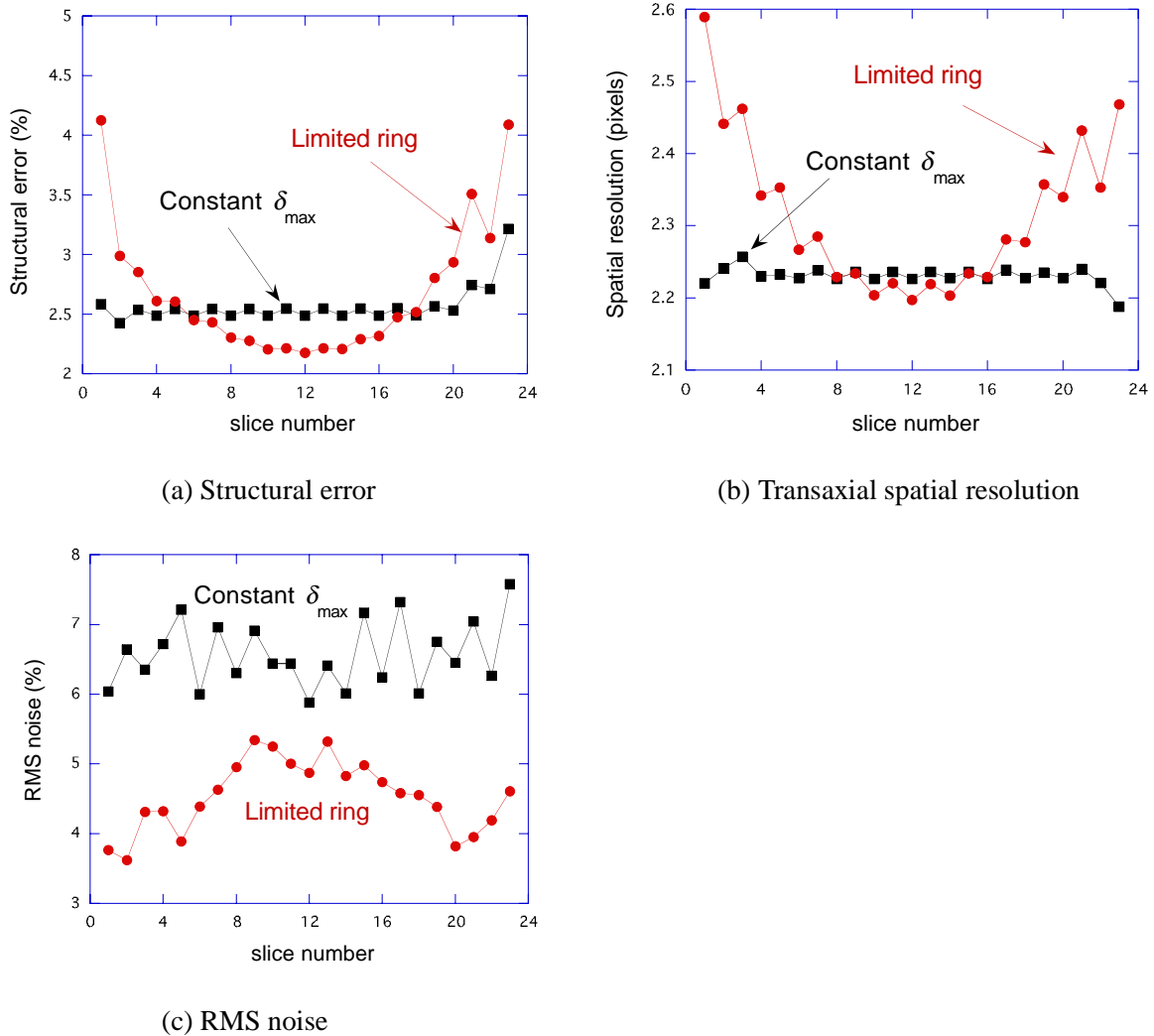
Figure 12. Comparisons of performances with limited detector ring and with constant δ_{max} after one main iteration. The number of detector rings is 12 and δ_{max}=6 in the constant δ_{max} test.

4. Discussion and conclusions

We have presented the theory of DRAMA-3D and the results of the simulation studies. The optimal relaxation parameter $\lambda(\delta, r)$ is given by equation (20) or (24), and its value is a function of the ring difference δ and the access order r of subsets. The δ-dependence plays an important role for providing uniform noise propagation in any mode of data access. As a result, DRAMA-3D is robust for various data access modes, and is suitable to achieve one-pass reconstruction. The parameters β_0 and $\beta(\delta)$ in equation (20) are determined by simple formulas (equations (11) and (17), respectively) from the parameters of the PET scanner, the operating conditions and the post smoothing resolution.

The damping factor α (≥ 1) is introduced to avoid instability, which may occur when the data having large δ are accessed at the early stage (small r) of iterations. It is preferable to take the α-value as small as possible to obtain faster convergence, but we have no theoretical means to determine the appropriate α-value, and we have to determine it experimentally for the particular operating conditions. However, if we first access the data having $\delta \leq 1$, DRAMA-3D provides stable convergence with $\alpha = 1$ regardless of the following access order for the remaining data having $\delta \geq 2$. We have confirmed this feature using $\lambda(\delta, r)$ defined by equation (24) with $\alpha = 1$. The reason for the stable convergence is that, after processing with $\delta \leq 1$, the value of $\lambda(\delta, r)$ for the following processing becomes sufficiently small (see equation (24)). In addition, the whole frequency components of images are properly reconstructed by the processing with $\delta \leq 1$ and the following iterations are quite stable.

Since the relaxation parameter depends on the ring difference δ, DRAMA-3D does not satisfy the convergence conditions of Neto and De Pierro (2005). The algorithm aims at one pass (single iteration) reconstruction as referred in the paper title. In fact, DRAMA-3D provides images having good noise balance (uniform noise propagation) by one or two main iteration(s). Our main concern is to realize a better noise balance with a single main iteration and not to realize stable convergence with a large number of the main iterations.

We have compared the performances of DRAMA-3D with the simpler algorithms, DRAMA(β) and RAMLA(λ). RAMLA(λ) is generally poor as shown in figure 10 as long as one-pass reconstruction is considered. RAMLA(λ) with descending data access mode showed exceptionally good performances, which is comparable to that of DRAMA-3D. It may be, however, an accidental result occurred in particular system parameters and δ_{max}-value. On the other hand, DRAMA(β) provides unexpectedly good performances with the CIS or random mode, if a suitable β-value is used. The RMS noise of DRAMA(β) is close to that of DRAMA-3D, although the *NPR* is about 2.0. This behavior indicates that the r-dependence in $\lambda(\delta, r)$ plays a more important role than the δ-dependence. However, the suitable β-value for DRAMA(β) depends sensitively on the operating conditions and data access mode, and it is generally not easy to find the suitable β-value in clinical routine. This will be a serious drawback of DRAMA(β).

In conclusion, we have developed a 3D-reconstruction algorithm, DRAMA-3D, for 3D-PET, and we have derived the optimal relaxation parameters suitable for one-pass image reconstruction. We have demonstrated the usefulness of the algorithm by simulation. In this study, however, we have made a lot of assumptions and approximations in the theory and in the simulation. For example, we have ignored attenuation and scattering of photons and the effect of random coincidence for simplicity. The sensitivity response of the detectors has also been simplified. Further work would be necessary to clarify the effect of these assumptions or approximations on the optimal relaxation parameters and on the performance of the algorithm.

Appendix A. 3D-frequency response of oblique projection data

It is known that, according to projection-slice theorem in 3D, oblique projection data with oblique angle φ lacks information in a cone region in 3D frequency space $(\omega_x, \omega_y, \omega_z)$ as shown in figure A1. The corresponding 2D frequency response at each slice-z is obtained by taking the 1D inverse Fourier transform of the 3D response with respect to the axial frequency ω_z. Consequently, at each slice-z, it is shown that information of low-frequency component (with small $\omega_x^2 + \omega_y^2$) is missing.
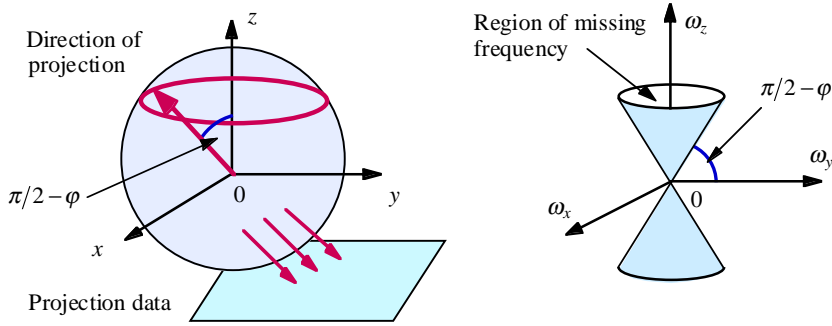
Figure A1. Relation between oblique projections (left) and the 3D Fourier transform (right)

Appendix B. Derivation of equation (15)

Consider the intersections between the two oblique LORs and the slice as shown in figure 1(b). We denote these two intersections by LOR-1 and LOR-2. The 2D "Gaussian" responses of the LOR-1 and LOR-2 are given by

$$Gau_1(\xi, \psi) = \exp\left\{-\frac{u^2}{2\sigma_s^2} - \frac{(v - v_0)^2}{2\sigma_0^2}\right\} \text{ and } Gau_2(\xi, \psi) = \exp\left\{-\frac{u'^2}{2\sigma_s^2} - \frac{(v' - v_0')^2}{2\sigma_0^2}\right\} \tag{B.1}$$

respectively, where (u, v) and (u', v') are the coordinates rotated by angle $\pm\theta(=\phi/2)$ with respect to the coordinates (ξ, ψ) around the origin of (ξ, ψ) as shown in figure B1. The coordinates of the centers of LOR-1 and LOR-2 are $(0, v_0)$ and $(0, v_0')$, respectively. The GCC between the two LORs crossing with azimuthal angle ϕ is expressed as

$$g(\delta, \phi) = \iint \iint Gau_1(\xi, \psi) Gau_2(\xi, \psi) \, d\xi \, d\psi \, dv_0 \, dv_0' \tag{B.2}$$

where the ranges of integration with the four variables are from $-\infty$ to $+\infty$. Equation (B.2) is however too complicated to execute the integration. We then intend to find a suitable approximate expression of the GCC in the followings.

If σ_0 is sufficiently large, the GCC given by equation (B.2) should be approximated by the GCC of the 2D-PET model given by (Tanaka and Kudo 2003)

$$g(\phi) = c \int_{-D/2}^{+D/2} \int_{-\infty}^{+\infty} \exp\left\{-\frac{\left(\xi_\theta - \xi\right)^2 + \left(\xi_\theta + \xi\right)^2}{2\sigma_\theta^2}\right\} d\xi\, d\psi \tag{B.3}$$

where $\theta = \phi/2$, $\xi_\theta = \psi\tan\theta$, $\sigma_\theta = \sigma_s/\cos\theta$, D is the diameter of the transaxial field of view, and c is the normalizing constant. The value of $g(\phi)$ is inversely proportional to $\sin\phi$ as shown by equation (9), and the value of $g(\phi)$ with a smaller ϕ affects more strongly to the value of the relaxation parameter $\lambda(\phi)$ than a smaller ϕ (see equation (5)). Taking into account this property, we intend to modify equation (B.3) so as to include the effect of the practical finite σ_0-value in the 3D-PET model. If ϕ is sufficiently small, the response of the GCC $g(\delta,\phi)$ in ψ-direction is approximated by the auto-correlation function of the Gaussian function (having standard deviation σ_0) due to the integration with respect to v_0 and v_0' in equation (B.2). The auto-correlation function is also a Gaussian function having the standard deviation $\sqrt{2}\sigma_0$. We then modify equation (B.3) by multiplying a 2D weighting factor $W(\xi,\psi)$ given by

$$W(\xi,\psi) = \exp\left\{-\left(\xi^2 + \psi^2\right)/(4\sigma_0^2)\right\}. \tag{B.4}$$

The function $W(\xi,\psi)$ is circularly symmetric, and the radial response of $W(\xi,\psi)$ is equal to the auto-correlation function. The reason why we use a circularly symmetric weighting factor is to simplify the following calculation. Thus, we obtain equation (15).

$$g(\delta,\phi) = c \int_{-\infty}^{+\infty} \int_{-\infty}^{+\infty} \exp\left\{-\frac{\left(\xi_\theta - \xi\right)^2 + \left(\xi_\theta + \xi\right)^2}{2\sigma_\theta^2}\right\} \exp\left(-\frac{\xi^2 + \psi^2}{4\sigma_0^2}\right) d\xi\, d\psi. \tag{15}$$

Equation (15) has been derived using intuitive or experienced approximations, and we have no evidence to guarantee the validity. The adequacy of equation (15) is evaluated by how it satisfies the following requirements: 1) the equation should be reduced to a simple analytical expression with reasonable approximations, 2) the resulted GCC should be consistent with the GCC of the 2D-PET model, 3) the GCC should be consistent with the concept of "CT-loss" in the 3D-PET model, 4) the relaxation parameter based on the GCC should provide good performance for DRAMA-3D regardless of the order of data access, and 5) the DRAMA-3D should provide uniform noise propagation regardless of the order of data access. It will be shown in this paper that the GCC given by equation (15) is fairly adequate because it satisfies the above requirements reasonably.
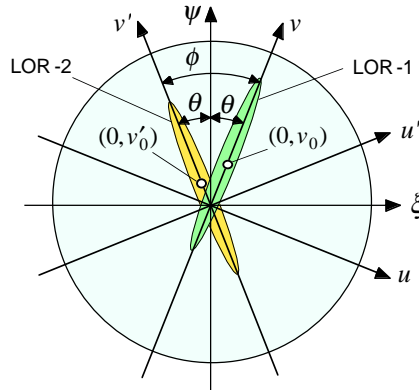
Figure B1. Gaussian intersections LOR-1 and LOR-2.

Appendix C. Derivation of equation (16)

We have, from equation (15)

$$g(\delta,\phi) = c\int_{-\infty}^{+\infty}\int_{-\infty}^{+\infty}\exp\left\{-\frac{\xi_\theta^2+\xi^2}{\sigma_\theta^2}-\frac{\xi^2+\psi^2}{4\sigma_0^2}\right\}\mathrm{d}\xi\,\mathrm{d}\psi$$

$$= c\int_{-\infty}^{+\infty}\int_{-\infty}^{+\infty}\exp\left\{-\left(\frac{\tan^2\theta}{\sigma_\theta^2}+\frac{1}{4\sigma_0^2}\right)\psi^2-\left(\frac{1}{\sigma_\theta^2}+\frac{1}{4\sigma_0^2}\right)\xi^2\right\}\mathrm{d}\xi\,\mathrm{d}\psi$$

$$= c\int_{-\infty}^{+\infty}\int_{-\infty}^{+\infty}\exp\left\{-\left(\frac{\sin^2\theta}{\sigma_s^2}+\frac{1}{4\sigma_0^2}\right)\psi^2-\left(\frac{\cos^2\theta}{\sigma_s^2}+\frac{1}{4\sigma_0^2}\right)\xi^2\right\}\mathrm{d}\xi\,\mathrm{d}\psi. \tag{C.1}$$

If we denote

$$\sigma_1 = \frac{1}{\sqrt{2}}\left(\frac{\sin^2\theta}{\sigma_s^2}+\frac{1}{4\sigma_0^2}\right)^{-1/2} \quad\text{and}\quad \sigma_2 = \frac{1}{\sqrt{2}}\left(\frac{\cos^2\theta}{\sigma_s^2}+\frac{1}{4\sigma_0^2}\right)^{-1/2} \tag{C.2}$$

then

$$g(\delta,\phi) = 4\pi c\sigma_1\sigma_2. \tag{C.3}$$

From equations (C.2) and (C.3),

$$g(\delta,\phi) = 4\pi c\left(\frac{4\sigma_s^4\sigma_0^4}{\left(4\sigma_0^2\sin^2\theta+\sigma_s^2\right)\left(4\sigma_0^2\cos^2\theta+\sigma_s^2\right)}\right)^{1/2}$$

$$= 4\pi c\left(\frac{4\sigma_s^4\sigma_0^4}{4\sigma_0^4\sin^2\phi+4\sigma_s^2\sigma_0^2+\sigma_s^4}\right)^{1/2}. \tag{C.4}$$

We determine the normalizing constant c so as to $g(\phi)=1$ when $\theta=0$.   We then have

$$g(\delta,\phi) = \left(\frac{4\sigma_s^4\sigma_0^4+\sigma_s^4}{4\sigma_0^4\sin^2\phi+4\sigma_s^2\sigma_0^2+\sigma_s^4}\right)^{1/2} \approx \left(\frac{\sigma_s^2}{\sigma_0^2\sin^2\phi+\sigma_s^2}\right)^{1/2} \quad\text{for}\quad 4\sigma_0^2 \gg \sigma_s^2. \tag{C.5}$$

Using equation (C.5) in equation (14.1), we have

$$\frac{1}{\beta(\delta)} = 2\int_{\Delta\phi}^{\pi/2}g^2(\delta,\phi)\mathrm{d}\phi = \frac{2\sigma_s}{\sqrt{\sigma_0^2+\sigma_s^2}}\left\{\frac{\pi}{2}-\arctan\left(\frac{\sqrt{\sigma_0^2+\sigma_s^2}}{\sigma_s}\tan\Delta\phi\right)\right\}. \tag{C.6}$$

Equation (C.6) gives the relation between $\beta(\delta)$ and $\Delta\phi$.

   Equation (C.6) corresponds to equation (10) in the 2D-PET model.   From equations (8) and (11), we have $\beta_0\Delta\phi = 2$, which is considered to be an expression of the consistency condition.   Assuming the similar consistency condition $\beta(\delta)\Delta\phi = 2$ is hold in the 3D-PET model, we can determine $\beta(\delta)$ from equation (C.6) by numerical calculation.   The obtained result is

$$\beta(\delta) = 1.04\sqrt{\sigma_0^2+\sigma_s^2}\big/\sigma_s. \tag{C.7}$$

We shall omit the factor 1.04 for simplicity in the following, since $\beta(\delta)\Delta\phi = 2$ is not a rigorous requirement.   We then have equation (16).

References

Browne J and De Pierro A 1996 A row-action alternative to the EM algorithm for maximizing likelihoods in emission tomography *IEEE Trans. Med. Imag.* **15** 687-99

Fukano A, Nakayama T and Kudo H 2004 Performance evaluation of relaxed block-iterative algorithms for 3-D PET reconstruction *Conf. Record of 2004 IEEE Medical Imaging Conference*, (M4-1) 2830-2834

Helou Neto E S and De Piero A R 2005 Convergence results for scaled gradient algorithms in positron emission tomography *Inverse Problems* **21** 1905-14

Hudson H M and Larkin R S 1994 Accelerated image reconstruction using ordered subsets of projection data *IEEE Trans. Med. Imag.* **13** 601-9

Meikle S R, Hutton B F, Bailey D L, Hooper P K and Fulham M J 1994 Accelerated EM reconstruction in total-body PET: potential for improving tumour detectability *Phys Med Biol* **39** 1689-704

Nakayama T and Kudo H 2005 Derivation and implementation of ordered-subsets algorithms for list-mode PET data *Conf. Record of 2005 IEEE Medical Imaging Conference*, (M05-7) 1950-1954

Natterer F 1986 *The mathematics of computerized tomography* (New York: Wiley)

Shepp L A and Vardi Y 1982 Maximum likelihood reconstruction for emission tomography *IEEE Trans. Med. Imag.* **1** 113-22

Snyder D L and Miller M I 1985 The use of sieves to stabilized images produced with the EM algorithm for emission tomography *IEEE Trans. Nucl. Sci.* **32** 3864-72

Tanaka E and Amo Y 1998 A Fourier rebinning algorithm incorporating spectral transfer efficiency for 3D PET *Phys. Med. Biol.* **43** 739-746

Tanaka E and Iinuma T 1976 Correction functions and statistical noise in transverse section picture reconstruction *Comput. Biol. Med.* **6** 295-306

Tanaka E and Kudo H 2003 Subset-dependent relaxation in block-iterative algorithms for image reconstruction in emission tomography *Phys. Med. Biol.* **48** 1405-1422

Tanaka E, Ote K, Isobe T, Watanabe M and Yamashita T 2007 A fast statistical image reconstruction algorithm for TOF-PET using DRAMA (Dynamic RAMLA) strategy *Conf. Record of 2007 IEEE Medical Imaging Conference*, (M19-215) 3850-3854

Yamada Y, Kitamura K, Hashizume N, Yamakawa Y and Kumazawa Y 2007 Reconstruction of 4-layer DOI detector equipped C-shaped PEM via list-mode iterative algorithm *Conf. Record of 2007 IEEE Medical Imaging Conference*, (M26-212) 4397-4400